Progress In Electromagnetics Research M, Vol. 111, 209–219, 2022

Switchable Active Metasurface for Dual Band Gain Enhancement

Arun Shaji* **and Anju Pradeep**

Abstract—A novel active metasurface which is switchable to accomplish dual band gain enhancement is reported. The metasurface is used as a superstrate above the dual band patch antenna working at 2.4 GHz and 4.6 GHz. The gain of the antenna is enhanced by 3.5 dB at both frequencies. Switching between the frequencies is enabled by a p-i-n diode. When the p-i-n diode is in the OFF state, gain is enhanced at 2.4 GHz, while gain is reduced at 4.6 GHz. When the p-i-n diode is in the ON state, gain is enhanced at 4.6 GHz, but reduced at 2.4 GHz. The diode is controlled by biasing with a regulated DC source. The efficiency of the antenna is 70% at 2.4 GHz and 85% at 4.6 GHz. The simulated and measured results show good agreement. The distance between the antenna and the superstrate is 6 mm, which is 0.048λ at 2.4 GHz and 0.092λ at 4.6 GHz. This superstrate can be used in WLAN and Sub-6 GHz 5G applications.

1. INTRODUCTION

With the advent of modern communication, the gain of the antenna should be high to compensate for the free space losses and to attain long distance communication. This can be achieved by means of metasurface superstrates. Metasurfaces are formed by planar metamaterial unit cell arrays which can alter electromagnetic waves. Conventional metasurfaces are used in a variety of applications [1–5]. Non-periodic metasurfaces are used in the design of broad band antennas [1]. Broad band RCS reduction is achieved with non-resonant metasurfaces [2]. Multifunction metasurfaces based on polarisation sensitivity are used in achieving multiple functions like sidelobe reduction, high focusing efficiency, and high aperture efficiency [3]. Side lobe suppression is achieved in metalens antennas using amplitude and phase controllable metasurfaces [4]. A metasurface based linear to linear cross polarisation convertor is used in the 'ku' band [5]. High gain is achieved in Terahertz antennas using multilayer metasurface [6]. Metasurface can be passive or active based on the structural arrangement and the components involved in the design of the unit cell. Passive metasurface lacks reconfigurability, which is required for some intelligent applications. An active metasurface is a class of metasurface with active components in its unit cell arrays. This type of metasurface provides reconfigurability, by controlling active components with external circuits and is used for adaptive applications [7, 8]. Active self-tuning metasurfaces are used in absorbing broadband high power surface currents [7]. Smart metasurface, which has self-adaptive reprogramming functionalities, is used in beam modulation [8]. Reconfigurable active metasurface is used in controlling the gain enhancement by which desired gain enhancement is obtained [9]. A 3-D printed metasurface is used for the gain enhancement of horn antennas [10]. Metasurface is used in the gain enhancement of slotted patch antennas [11]. Wide band and multimode metasurfaces, which are used in gain enhancement, are significant in the design of 5G antennas [12]. Near-zero refractive index metasurface aids in enhancing the front to back radiation ratio by converging the electromagnetic waves [13].

Received 12 May 2022, Accepted 27 June 2022, Scheduled 18 July 2022

* Corresponding author: Arun Shaji (shaji87@gmail.com).
The authors are with the Division of Electronics, School of Engineering, Cochin University of Science and Technology, Cochin 682022, India.

Nonreciprocal dual polarised active metasurface aids in spacial wave amplification [14]. Self-configurable metasurface provides both gain enhancement and absorption at the same frequency [15]. Reconfigurable metasurface helps in shaping the beam of the antenna together with gain enhancement in different frequencies [16–18]. Bidirectional high gain patch antenna is created using a focusing metasurface, and the reflective focusing metasurface is used to create a wide band high gain patch [19, 20]. Due to the wide range of possibilities, there is a demand for metasurface that can work at multiple frequencies. The novelty of this paper is using switchable active metasurface for the gain enhancement of patch antennas at two resonant frequencies, 2.4 GHz and 4.6 GHz. The prototype of the proposed metasurface is fabricated, and experimental validations are carried out. This article is organized as follows. Section 2 explains the design of the metasurface unit cell. Section 3 deals with the design of the active metasurface, and Section 4 is about the measurement results and the discussion. Finally, the conclusion of the work is given in Section 5.

2. DESIGN OF ACTIVE METAMATERIAL UNIT CELL

2.1. Metamaterial Unit Cell

The design of the unit cell starts with the cross shaped structure as shown in Figure 1(a), which resonates at 5.6 GHz. To get dual bands of resonance, the structure is made on both sides of the FR4 substrate. The resonant frequency is reduced by increasing the electrical length of the cross shaped structure, forming an S-shaped structure. The structure now resonates at 2.4 GHz. A slit is introduced in the S-shaped structure to control the resonance between 2.4 and 4.6 GHz. The slit is replaced by a p-i-n diode, making the unit cell active and also enabling switching between the two frequencies. The S-shaped structures on the front and back sides of the unit cell with the p-i-n diode are shown in Figures 1(b) and (c). The unit cell is actively controlled to be in an ON state when the diode is biased and in an OFF state when the diode is unbiased.

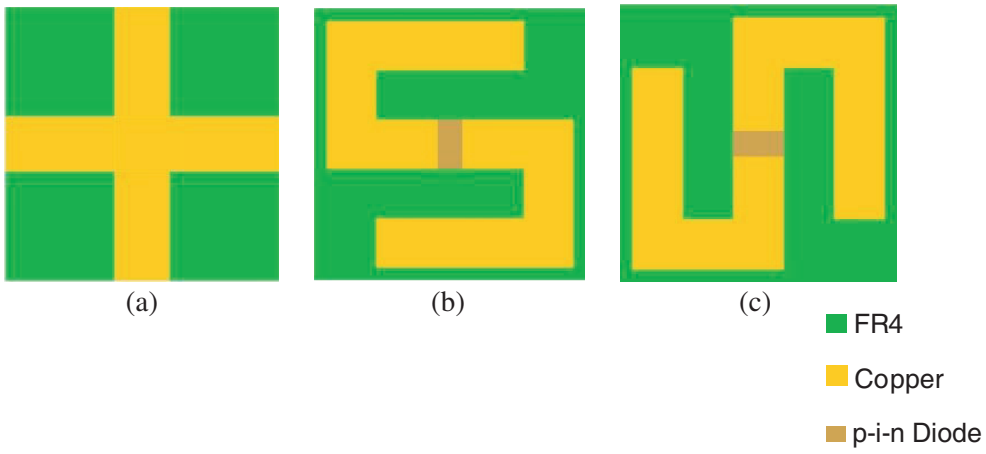

Figure 1. Design steps of the unit cell. (a) Cross shape. (b) 'S' shape Top view. (c) 'S' shape Bottom view.

The dimensions of the unit cell at the top and bottom sides are shown in Figures 2(a) and (b), in which λ represents the wavelength of the lowest frequency. The FR4 substrate has a permittivity of 4.4 and a loss tangent of 0.02. The thickness of the substrate is 1.6 mm. A Floquet port analysis of the unit cell is done, and the transmission and reflection characteristics are analysed. The magnitude of S_{21} in dB and the phase of the transmission characteristics of the unit cell are shown in Figure 3. The magnitude switches between 2.4 GHz and 4.6 GHz at ON and OFF conditions, respectively. The phase of the unit cell in the OFF condition is linear at 2.4 GHz, and the phase of the unit cell in the ON condition is linear at 4.6 GHz at which it aids transmission.

The p-i-n diode is modeled in HFSS using lumped components, based on the equivalent circuit of the p-i-n diode in biased and unbiased condition, as shown in Figure 4. The parameters of the p-i-n

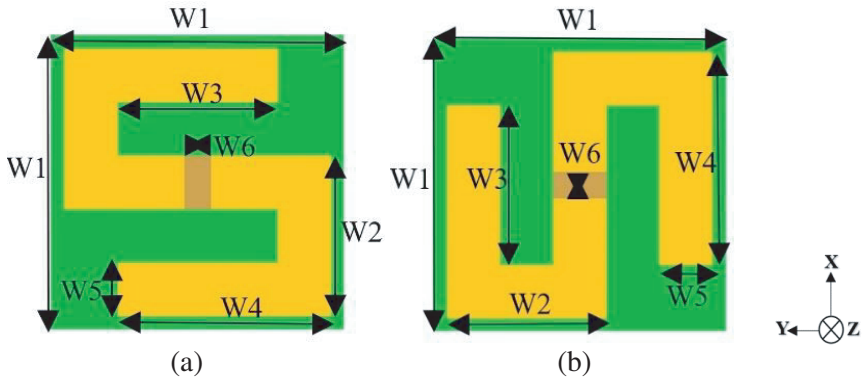

Figure 2. (a) Top view of the unit cell. (b) Bottom view ($W1 = 0.1144\lambda$, $W2 = 0.0624\lambda$, $W3 = 0.0624\lambda$, $W4 = 0.0832\lambda$, $W5 = 0.0208\lambda$, $W6 = 0.0104\lambda$).

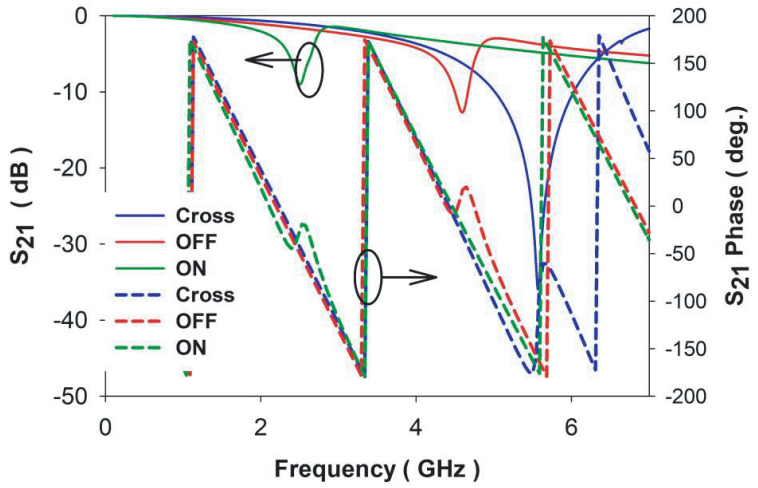

Figure 3. Transmission characteristics of the unit cell.

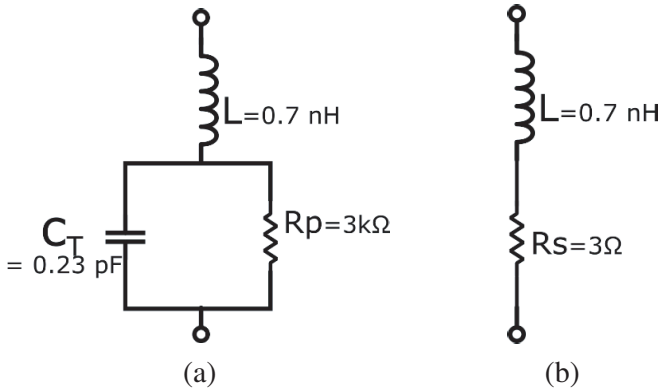

Figure 4. Equivalent circuit model of p-i-n diode. (a) Reverse bias. (b) Forward bias.

diode used for simulation are $L = 0.7\,\text{nH}$, ON resistance $R_s = 2\,\Omega$, OFF resistance $R_p = 3\,\text{k}\Omega$, OFF capacitance $C_p = 0.23\,\text{pF}$ [24].

When the p-i-n diode is in ON condition, the unit cell resonates at 2.4 GHz, and when the p-i-n diode is in OFF condition, it resonates the unit cell at 4.6 GHz.

The parameters of the unit cell are extracted from the scattering parameters using the following expressions. The impedance 'z' is obtained from the S parameters using Equation (1).

$$z = \pm\sqrt{\frac{(1+S_{11})^2 - S_{21}^2}{(1-S_{11})^2 - S_{21}^2}} \tag{1}$$

$$e^{ink_0d} = X \pm i\sqrt{1-X^2} \tag{2}$$

where 'k' represents the wave number, and 'd' represents the thickness of the metamaterial unit cell

$$X = \frac{1}{2S_{21}(1 - S_{11}^2 + S_{21}^2)} \tag{3}$$

Now the value of refractive index 'n' can be found using the following equation,

$$n = \frac{1}{k_0 d}\left[\ln\left(e^{ink_0d}\right)''\right] - i\left[\ln\left(e^{ink_0d}\right)'\right] \tag{4}$$

where $(.)'$ and $(.)''$ represent the real and imaginary values, respectively. Now the permeability can be calculated using the following equation

$$\mu = nz \tag{5}$$

where 'μ' is the permeability. The extracted parameters [21] of the unit cell are shown in Figure 5. In the ON state, the real value of the permeability crosses zero at 2.4 GHz and gives near-zero property at the same frequency, as shown in Figures 5(a)–(b). In OFF condition, the real value of the permeability

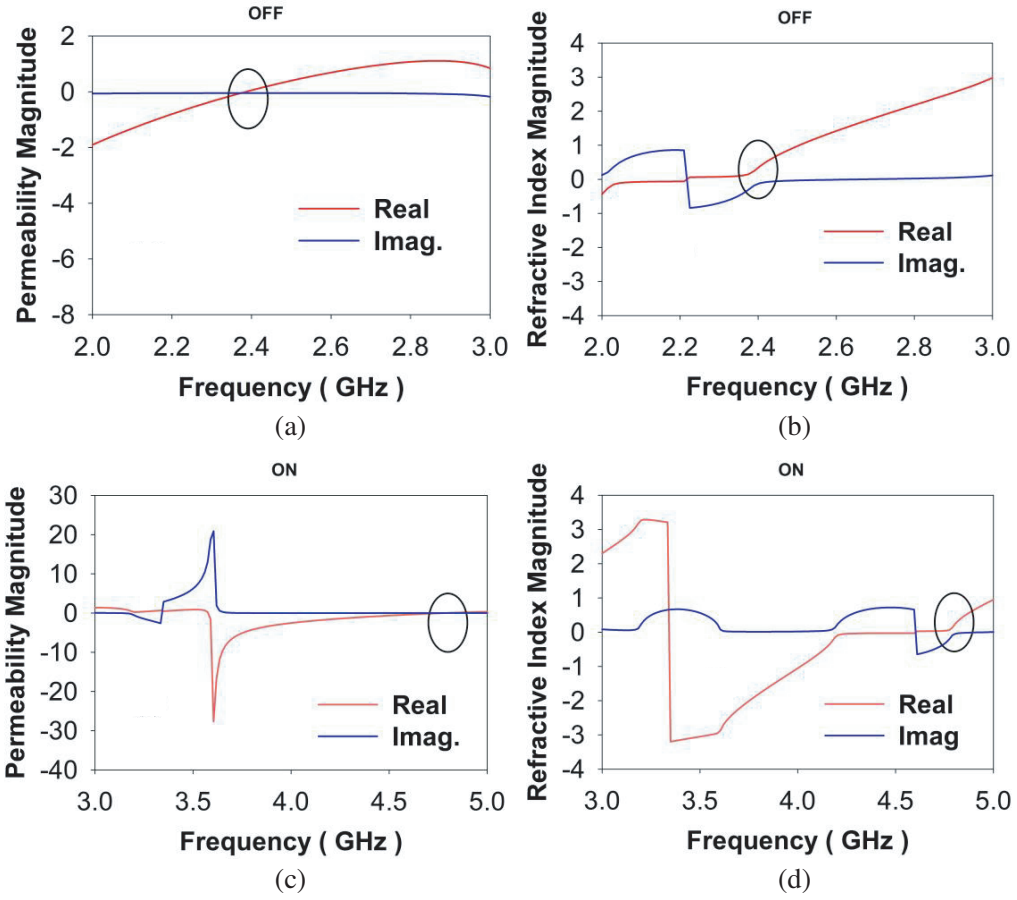

Figure 5. Extracted parameters of the unit cell. (a) Permeability in OFF condition. (b) Refractive index in OFF condition. (c) Permeability in ON condition. (d) Refractive index in ON condition.

crosses zero at 4.6 GHz, and a near-zero property is obtained at the same frequency as shown in Figures 5(c)–(d). In both cases, the real refractive index is near-zero, and the imaginary one approaches from negative to zero, which enhances the gain [22] of the antenna.

3. DESIGN OF ACTIVE METASURFACE

The metasurface is initially formed by a 2 × 2 unit cell on an FR4 substrate. The ON condition and OFF condition are obtained by connecting the p-i-n diode in the slit on the S-shaped structure on both sides of the substrate. The MS superstrate is designed on a 104 mm × 104 mm substrate, which is the same as the size of the ground plane of a patch antenna. To enhance the performance of the antenna, the array size of the metasurface is further increased. The metasurface is formed by 4 × 4-unit cells on the same FR4 substrate. The metasurface is kept above the patch antenna working at dual frequencies, 2.4 GHz and 4.6 GHz. The reference antenna is a rectangular patch antenna, which is designed on an FR4 substrate with a relative permittivity of 4.4, loss tangent of 0.02, and thickness of 1.6 mm. It has a peak gain of 3 dBi at 2.4 GHz and 4.5 dBi at 4.6 GHz. The three-dimensional geometry of the proposed antenna with the metasurface and the reference patch antenna is shown in Figure 6. A single layer metasurface is used for the gain enhancement at 2.4 GHz and 4.6 GHz, making the metasurface applicable to dual-frequencies. The gain enhancement is switched between the two frequencies using the p-i-n diode control. The height between the antenna and the superstrate is optimized as 6 mm from the antenna, at which gain enhancement is achieved at both frequencies.

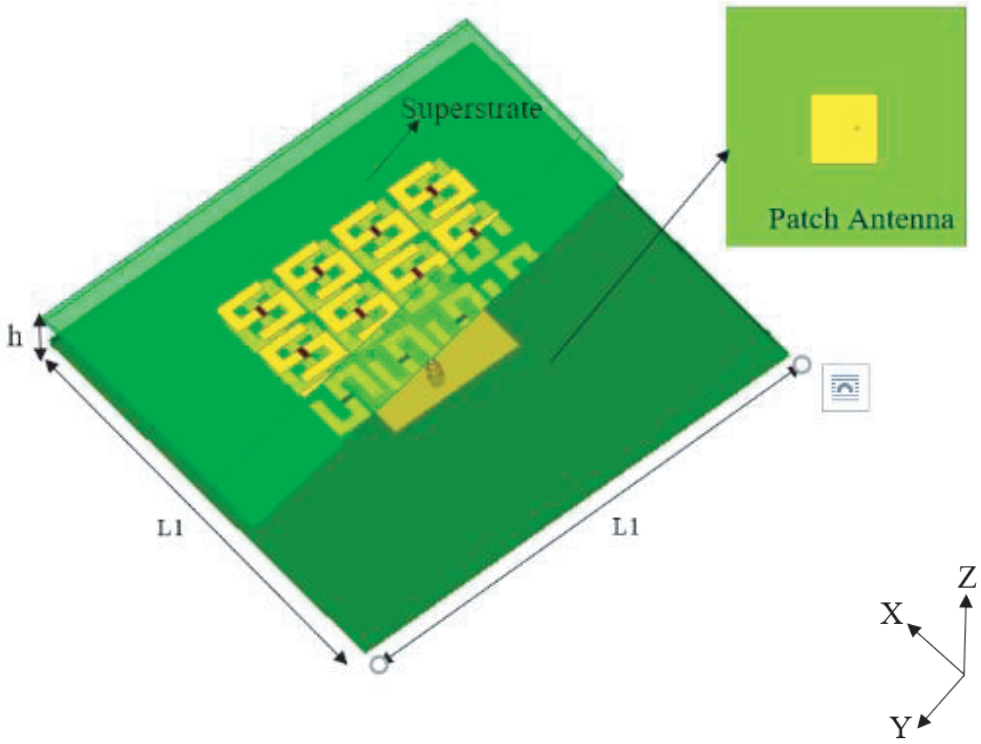

Figure 6. 3-D geometry of the proposed structure ($L1 = 104$ mm, $h = 6$ mm).

4. MEASUREMENT RESULTS AND DISCUSSION

The antenna with a metasurface superstrate is measured using the Anritsu MS46122B Vector Network Analyzer. The simulated and measured reflection characteristics of the antenna with and without metasurface superstrate are shown in Figure 7. The simulated and measured results show good agreement at 2.4 GHz, while the measured reflection characteristics at 4.6 GHz is slightly different from

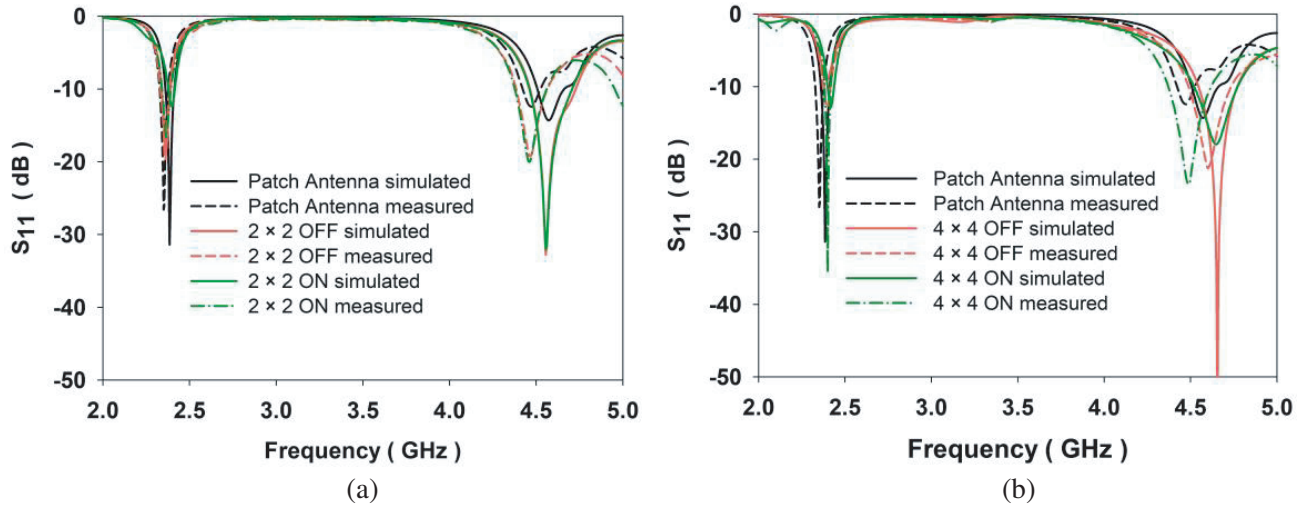

Figure 7. Reflection characteristics of the antenna. (a) 2×2 array. (b) 4×4 array.

the simulated results. This may be due to fabrication inaccuracies and soldering defects. The p-i-n diodes in the superstrate are switched ON and OFF using DC biasing. The PIN diode used is SMP 1320-079LF with the SC79 package, which has a forward voltage of 0.85 V. The measurement is done for two types of metasurfaces, one with a 2×2-unit cell array and the other with a 4×4-unit cell array. The 2×2-unit cellarray gives a gain enhancement of 1.5 dB at 2.4 GHz, when the diodes are OFF and a gain enhancement of 1.5 dB at 4.6 GHz, when the diodes are ON. The 4×4 array metasurface enhances the gain by 3.5 dB at 2.4 GHz and 4.6 GHz under OFF and ON conditions, respectively. The gain at the other frequency decreases, thereby contributing more to the desired frequency. The measured gain versus frequency plot of the patch antenna and the antenna with metasurface is shown in Figure 8(a). The gain of the antenna is analyzed by varying the height between the antenna and superstrate. The optimum gain at both frequencies is obtained at a distance of 6 mm. The variation of the gain with respect to height is shown in Figure 8(b). The peak gain of the antenna increased to 6.5 dBi at 2.4 GHz and 8 dBi at 4.6 GHz.

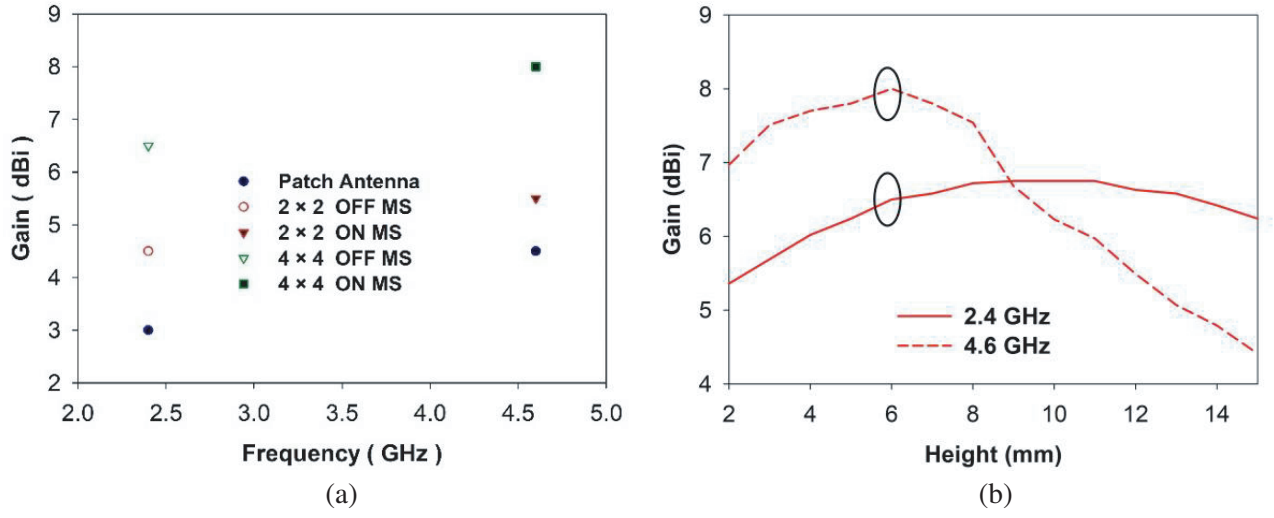

Figure 8. (a) Measured gain vs frequency. (b) Height vs gain.

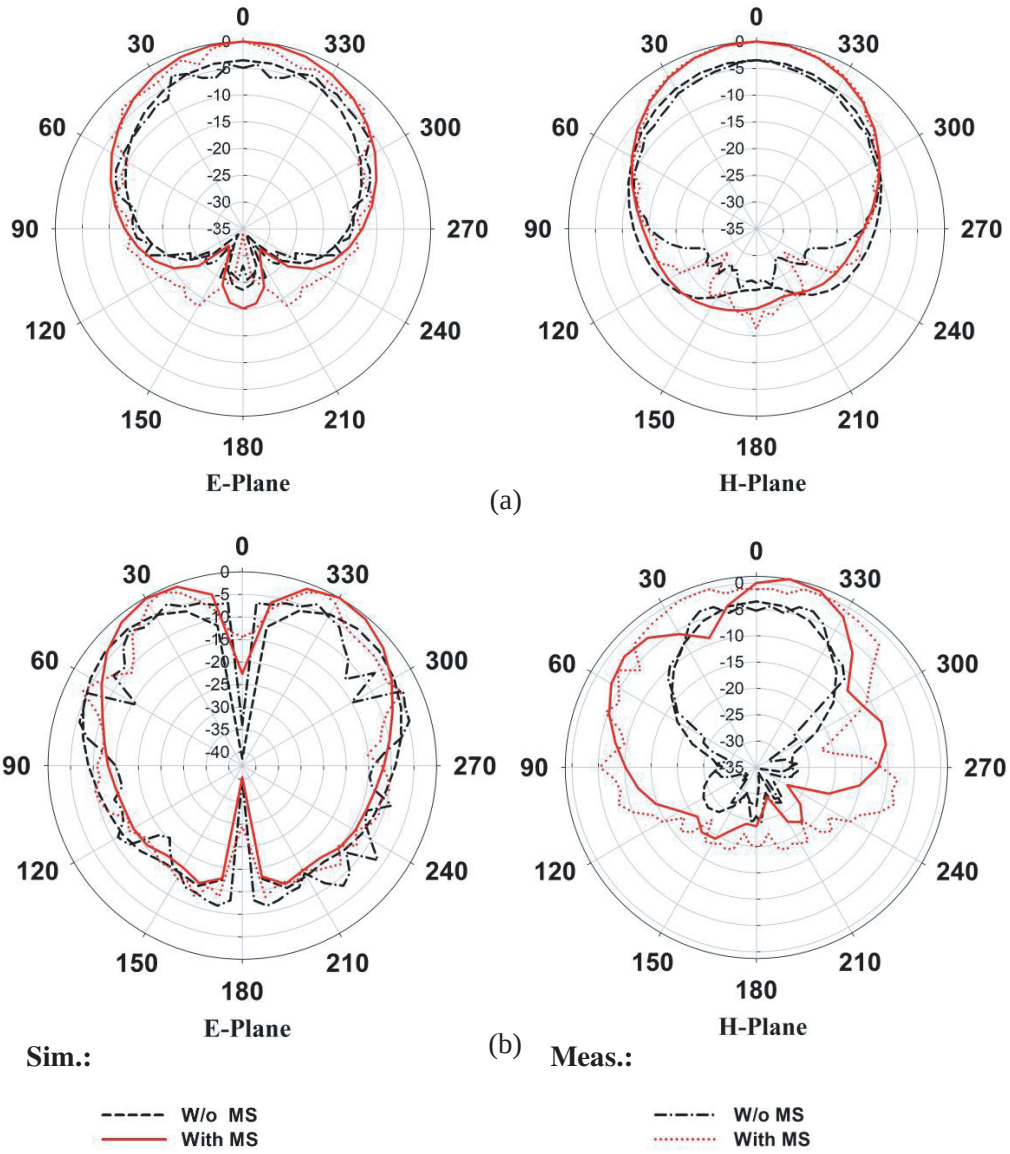

Figure 9. Simulated and measured radiation pattern in E and H plane. (a) 2.4 GHz. (b) 4.6 GHz.

The radiation patterns of the antenna with and without an OFF condition metasurface in the E-plane and H-plane at 2.4 GHz are shown in Figure 9(a). It can be seen that the directionality of the antenna with metasurface has increased. The metasurface has reduced the beamwidth by 5° in the E-plane and reduced the beam width by 9° in the H-plane. The radiation patterns of the antenna with and without ON condition metasurface in the E-plane and H-plane at 4.6 GHz are shown in Figure 9(b). The metasurface has reduced the beamwidth by 50° in the E-plane and 61° in the H-plane.

The radiation efficiency [23] of the antenna is expressed as (6)

$$\eta = \frac{R_r}{R_r + R_L} \tag{6}$$

where 'η' represents the radiation efficiency, 'R_r' the radiation resistance, and 'R_L' the loss resistance of the antenna. The radiation efficiency of the patch antenna with superstrates is shown in Figure 10. The efficiency of the patch antenna is 40% at 2.4 GHz and 50% at 4.6 GHz. The superstrate in the OFF condition increases the efficiency to 70% at 2.4 GHz, and the superstrate in the ON condition increases the efficiency to 85%.

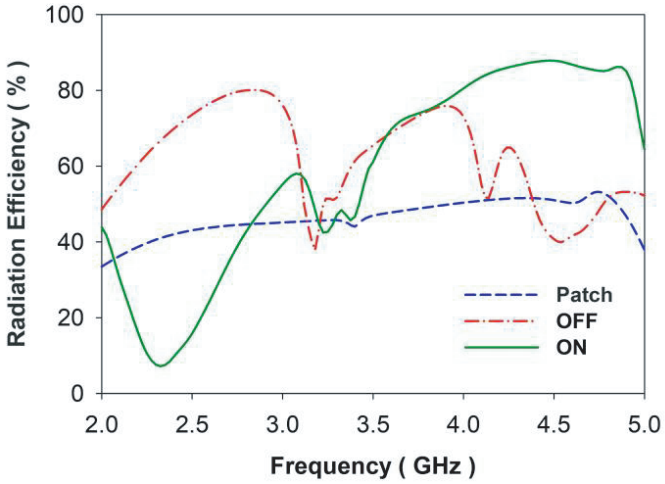

Figure 10. Efficiency vs frequency.

The distance between the patch antenna and metasurface is 6 mm at both frequencies. The measurement setup for antenna measurements is shown in Figure 11(a), and the prototype of the fabricated structures with the connected diodes and the reference antenna are shown in Figures 11(b), (c), and (d).

The comparisons of our work with the previous works are done and shown in Table 1. The distance between the antenna and the superstrate of the proposed antenna is 0.048λ at 2.4 GHz and 0.092λ at 4.6 GHz, where λ is the free space wavelength. This reduces the bulkiness of the antenna. This work gives gain enhancement at two frequencies, which is switchable. Switching is obtained using a p-i-n diode, an active component which is properly biased to give gain enhancement at one frequency at a time, while the gain at the other frequency is reduced. This makes our work different from the other reported works. A single layer superstrate is used, which gives selective gain enhancement. Frequency switching with 3.5 dB gain enhancement is higher than the previous works.

Table 1. Comparison of this work with other Antennas.

Ref.	Height between antenna and superstrate	Operating frequency	Gain Enhancement	Frequency switching	Type of Metasurface	No. of layers
[9]	0.29 λ	10.44 GHz	2.27 dB	-	Active, p-i-n diode	1
[17]	0.55 λ	4.6 GHz	4.5 dB	-	Active, Schottky diode	1
[19]	0.64 λ	5.3 GHz, 6.6 GHz	2 dB	yes	Active, Varactor diode	2
[20]	0.11 λ	1.85 GHz–2.25 GHz	6 dB	-	Active, Varactor diode	1
This work	**0.048 λ**	**2.4 GHz, 4.6 GHz**	**3.5 dB**	**yes**	**Active, p-i-n diode**	**1**

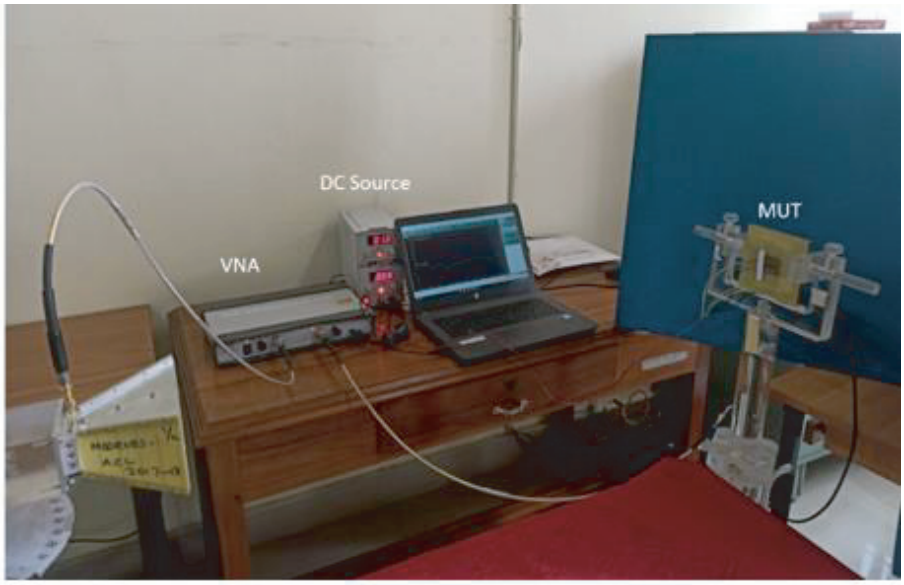

(a)

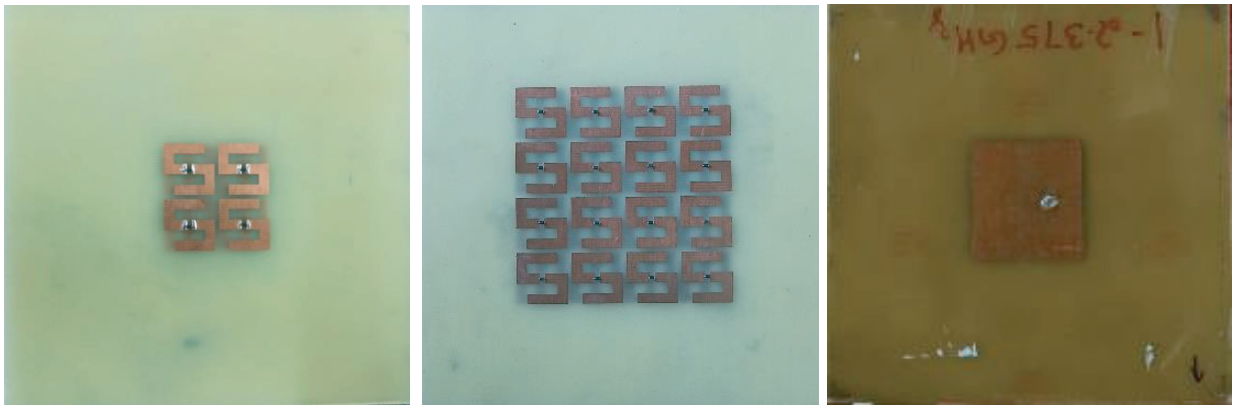

(b) (c) (d)

Figure 11. Measurement setup and the fabricated structures. (a) Measurement setup. (b) Superstrate with 2×2 unit cell. (c) Superstrate with 4×4 unit cell. (d) Patch antenna.

5. CONCLUSION

A switchable active metasurface for gain enhancement is proposed for dual frequencies. Gain enhancement of 3.5 dB is obtained at 2.4 GHz and 4.6 GHz. Switching between the frequencies is done by properly biasing the p-i-n diodes, by which gain enhancement at one frequency is obtained at a time. The simulated and measured results show good agreement. This superstrate can be used to improve WLAN gain at 2.4 GHz and 5G applications operating in the sub-6 GHz band of 4.5 GHz–4.9 GHz. Switching can be automated with the help of microcontrollers and can be applied to antennas with automatic switching systems.

REFERENCES

1. Liu, S., D. Yang, Y. Chen, K. Sun, X. Zhang, and Y. Xiang, "Low-profile broadband metasurface antenna under multimode resonance," *IEEE Antennas and Wireless Propagation Letters*, Vol. 20, No. 9, 1696–1700, 2021.

2. Wang, Y., K. Chen, Y. Li, and Q. Cao, "Design of nonresonant metasurfaces for broadband RCS reduction," *IEEE Antennas and Wireless Propagation Letters*, Vol. 20, No. 3, 346–350, 2021.
3. Huang, H.-F. and J. Zhang, "High-efficiency multifunction metasurface based on polarization sensitivity," *IEEE Antennas and Wireless Propagation Letters*, Vol. 20, No. 8, 1508–1512, 2021.
4. Lou, Q. and Z. N. Chen, "Sidelobe suppression of metalens antenna by amplitude and phase controllable metasurfaces," *IEEE Transactions on Antennas and Propagation*, Vol. 69, No. 10, 6977–6981, 2021.
5. Su, J., Y. Guo, X. Chen, and W. Zhang, "A dual-wideband polarization-insensitive linear polarization converter based on metasurface," *Progress In Electromagnetics Research M*, Vol. 108, 213–222, 2022.
6. Khajeh-Khalili, F. and Y. Dohni-Zadeh, "High-gain multi-layer antenna using metasurface for application in terahertz communication systems," *Int. J. Electron. Device Phys.*, Vol. 4, 007, 2020.
7. Kim, S., A. Li, J. Lee, and D. F. Sievenpiper, "Active self-tuning metasurface with enhanced absorbing frequency range for suppression of high-power surface currents," *IEEE Transactions on Antennas and Propagation*, Vol. 69, No. 5, 2759–2767, 2021.
8. Shrestha, S., A. A. Baba, S. M. Abbas, M. Asadnia, and R. M. Hashmi, "A horn antenna covered with a 3D-printed metasurface for gain enhancement," *Electronics*, Vol. 10, No. 2, 119, 2021.
9. Almizan, H., Z. A. A. Hassain, T. A. Elwi, and S. M. Al-Sabti, "Controlling gain enhancement using a reconfigurable metasurface layer," *12th International Symposium on Advanced Topics in Electrical Engineering (ATEE)*, 1–6, 2021.
10. Ma, Q., G. D. Bai, H. B. Jing, et al., "Smart metasurface with self-adaptively reprogrammable functions," *Light Sci. Appl.*, Vol. 8, No. 98, 2019.
11. Samantaray, D. and S. Bhattacharyya, "A gain-enhanced slotted patch antenna using metasurface as superstrate configuration," *IEEE Transactions on Antennas and Propagation*, Vol. 68, No. 9, 6548–6556, 2020.
12. Bai, H., G.-M. Wang, and X.-J. Zou, "A wideband and multi-mode metasurface antenna with gain enhancement," *AEU — International Journal of Electronics and Communications*, Vol. 126, 153402, 2020.
13. Dawar, P. and M. Abdalla, "Miniaturized dual-band embedded NZI metasurface antenna with front-to-back radiation ratio enhancement," *Progress In Electromagnetics Research B*, Vol. 95, 61–79, 2022.
14. Lou, T., X.-X. Yang, G. He, W. Che, and S. Gao, "Dual-polarized nonreciprocal spatial amplification active metasurface," *IEEE Antennas and Wireless Propagation Letters*, Vol. 20, No. 9, 1789–1793, 2021.
15. Phon, R. and S. Lim, "Self-reconfigurable dual-mode metasurface," *IEEE International Symposium on Antennas and Propagation and North American Radio Science Meeting*, 885–886, 2020.
16. Zhang, J., Y. Liu, Y. Jia, and R. Zhang, "High-gain Fabry-Pérot antenna with reconfigurable scattering patterns based on varactor diodes," *IEEE Transactions on Antennas and Propagation*, Vol. 70, No. 2, 922–930, 2022.
17. Bai, L., X. G. Zhang, Q. Wang, C. X. Huang, W. X. Jiang, and T. J. Cui, "Dual-band reconfigurable metasurface-assisted Fabry-Pérot antenna with high-gain radiation and low scattering," *IET Microw. Antennas Propag.*, Vol. 14, 1933–1942, 2020.
18. Burokur, S. N., J. P. Daniel, P. Ratajczak, and A. de Lustrac, "Tunable bilayered metasurface for frequency reconfigurable directive emissions," *Appl. Phys. Lett.*, Vol. 97, 064101, 2010.
19. Zhou, E., Y. Cheng, F. Chen, and H. Luo, "Wideband and high-gain patch antenna with reflective focusing metasurface," *AEU — International Journal of Electronics and Communications*, Vol. 134, 153709, 2021.
20. Wang, J., Y. Cheng, H. Luo, F. Chen, and L. Wu, "High-gain bidirectional radiative circularly polarized antenna based on focusing metasurface," *AEU — International Journal of Electronics and Communications*, Vol. 151, 154222, 2022.

21. Chen, X., T. Grzegorczyk, B.-I. Wu, J. Pacheco, Jr., and J. A. Kong, "Robust method to retrieve the constitutive effective parameters of metamaterial," *Phys. Rev. E*, Vol. 70, 016608, 2004.
22. Chen, Y. F., P. Fischer, and F. W. Wise, "Negative refraction at optical frequencies in nonmagnetic two-component molecular media," *Phys. Rev. Lett.*, Vol. 95, No. 6, 067402, 2005.
23. Balanis, C. A., *Antenna Theory: Analysis and Design*, 4th Edition, John Wiley & Sons, 2016.
24. Skyworks, "SMP1320 Series: Low Resistance, Low Capacitance, Plastic Packaged PIN Diodes," 200047S, Nov. 2018.